Journal of Materials Chemistry A

RSC Publishing

PAPER

Highly stable nanoporous covalent triazine-based frameworks with an adamantane core for carbon dioxide sorption and separation†

Cite this: *J. Mater. Chem. A*, 2013, **1**, 14990

Asamanjoy Bhunia,[a] Ishtvan Boldog,[a] Andreas Möller[b] and Christoph Janiak*[a]

Adamantane substituted with two to four 4-cyanophenyl groups was used for preparation of a new series of robust Porous Covalent Triazine-based Framework (PCTF) materials. Novel adamantane PCTFs were synthesized in good yields (>80%) by the trimerization reaction of 1,3-bis-, 1,3,5-tris- and 1,3,5,7-tetrakis(4-cyanophenyl)adamantane, respectively, in the presence of $ZnCl_2$ (Lewis acid condition) and CF_3SO_3H (strong Brønsted acid condition). From N_2 adsorption isotherms, the Lewis acid condition gives higher surface areas than the strong Brønsted acid condition. The amorphous nano- to microporous frameworks (>50% micropore fraction) exhibit excellent thermal stabilities (>450 °C) with BET surface areas up to 1180 $m^2\ g^{-1}$. A very similar ultramicropore size distribution between 4 and 10 Å was derived from CO_2 adsorption isotherms with a "CO_2 on carbon based slit-pore model". At 1 bar the gases H_2 (at 77 K), CO_2 (at 273 and 293 K) and CH_4 (at 273 K) are adsorbed up to 1.24 wt%, 58 $cm^3\ g^{-1}$ and 20 $cm^3\ g^{-1}$, respectively. Gas uptake increases with BET surface area and micropore volume which in turn increase with the number of cyano groups in the monomer. From single component adsorption isotherms, IAST-derived ideal CO_2:N_2, CO_2:CH_4 and CH_4:N_2 selectivity values of up to 41 : 1, 7 : 1 and 6 : 1, respectively, are calculated for $p \rightarrow 0$ at 273 K. The adamantane PCTFs have isosteric heats of adsorption for CO_2 of 25–28 kJ mol^{-1} at zero loading and most of them also >25 kJ mol^{-1} over the entire adsorption range which is well above the heat of liquefaction of bulk CO_2 or the isosteric enthalpy of adsorption for CO_2 on activated carbons.

Received 28th August 2013
Accepted 9th October 2013

DOI: 10.1039/c3ta13407e

www.rsc.org/MaterialsA

Introduction

Design and synthesis of porous covalent organic frameworks (COFs) have attracted huge attention because of their potential applications in gas storage, separation, catalysis and optoelectronics.[1,2] COFs are constructed by linking well defined organic building units through covalent bonds (*e.g.*, C–C, C–N, C–O and B–O).[3,4] Compared with metal–organic frameworks (MOFs), COFs could demonstrate higher chemical stability, specific surface areas and building block variability. Covalent organic frameworks possess Brunauer–Emmett–Teller (BET) surface areas in the range of several hundreds to several thousands of $m^2\ g^{-1}$.[5] However, boronate based COFs are not stable against humidity even under ambient conditions, which make them difficult to use for gas storage applications.[6,7] Further, classes of porous organic frameworks are differentiated according to their building units such as benzimidazole-linked polymers (BILPs),[2] hyper-crosslinked polymers (HCPs),[8] polymers of intrinsic microporosity (PIMs),[9] porous aromatic frameworks (PAFs),[10,11] conjugated microporous polymers (CMPs)[12] and covalent triazine-based frameworks (CTFs).[13] BILPs are synthesized by metal-free co-condensation reactions involving arylaldehyde and *ortho*-diamine with surface areas of 708–1306 $m^2\ g^{-1}$.[2,14,15] HCPs have surface areas ranging from 330 to 2090 $m^2\ g^{-1}$ and require harsh synthetic conditions.[16,17] PAF-1 exhibits one of the highest BET surface areas of 5640 $m^2\ g^{-1}$ among organic frameworks.[10] Recently, Banerjee *et al.* synthesized Schiff based COFs with surface areas up to 535 $m^2\ g^{-1}$ by combining reversible and irreversible organic reactions.[5b]

Kuhn, Antonietti and Thomas *et al.* developed CTFs with permanent porosity.[13,18–21] CTFs are interesting because of advantages such as cheap and readily available starting materials, facile synthesis and a certain hydrophilicity. In addition, CTFs have been used in heterogeneous catalysis,[21] as a catalytic support in liquid phase reactions,[22] for gas storage,[23] and separation of organic dyes.[24] Recently, we reported the transformation of tetrakis(4-cyanophenyl)ethylene (**M1**) under Lewis acidic ($ZnCl_2$) conditions at 400 °C to porous covalent triazine-based frameworks (PCTF-1 and -2) with high surface area

[a]*Institut für Anorganische Chemie und Strukturchemie, Heinrich-Heine-Universität Düsseldorf, 40204 Düsseldorf, Germany. E-mail: janiak@uni-duesseldorf.de; Fax: +49-211-81-12287; Tel: +49-211-81-12286*

[b]*Institut für Nichtklassische Chemie e.V., Permoserstr. 15, D-04318 Leipzig, Germany*

† Electronic supplementary information (ESI) available: Syntheses, XRD, CHN, TGA, gas uptake and selectivity of PCTFs. See DOI: 10.1039/c3ta13407e

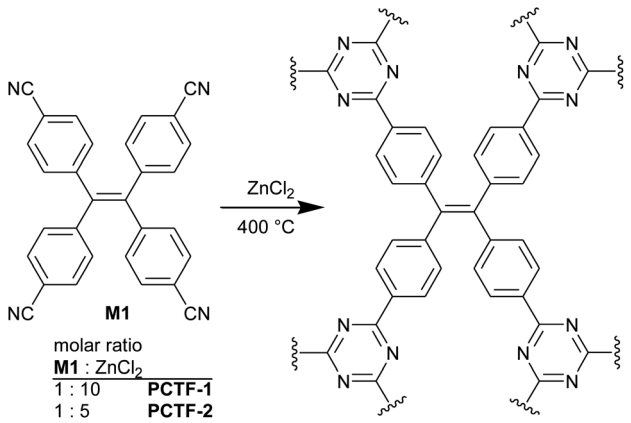

Scheme 1 Synthesis of PCTF-1 and -2.

(2235 $m^2 g^{-1}$), high CO_2, CH_4 and H_2 uptake for a CTF material (1.86 wt% H_2 at 77 K, 1 bar) (Scheme 1).[23]

Here we introduce three adamantane substituted nitriles 1,3-bis-, 1,3,5-tris- and 1,3,5,7-tetrakis(4-cyanophenyl)adamantane (**M2–M4**, Scheme 2) as new monomer motifs for PCTF preparation. The rigid tetrahedral adamantane core and the phenyl spacers between the core and the nitrile groups may help to increase the available space accessible for gas adsorption and storage. We report the synthesis of five adamantane based CTFs by using both Lewis acid ($ZnCl_2$) and strong Brønsted acid (CF_3SO_3H) conditions and examine their gas (H_2, CO_2 and CH_4) storage capacities and selective CO_2 binding over N_2 and CH_4. From their elemental composition (see below) we view CTFs from ionothermal reaction with $ZnCl_2$ in-between well-defined COFs and porous carbon materials. The latter are key materials,[25] *inter alia* as sorbents for separation processes and gas storage.[26]

Results and discussion

Porous CTF materials can be synthesized by an ionothermal reaction between aromatic nitriles in $ZnCl_2$ which can be adapted to a large scale. Molten $ZnCl_2$ acts as a Lewis acid catalyst, molten solvent and porogen for the polymerization. A trimerization

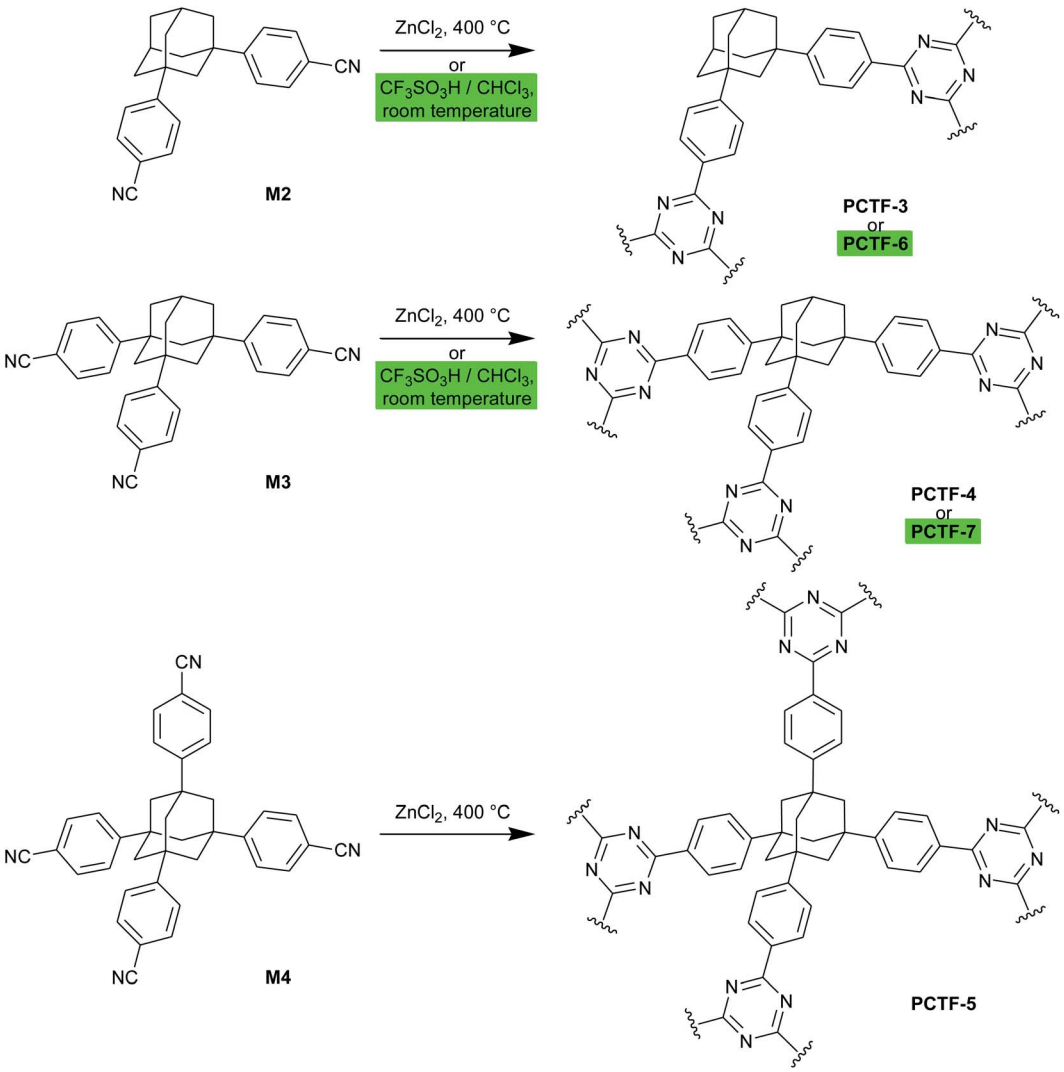

Scheme 2 Synthesis of porous covalent triazine-based frameworks PCTF-3 to PCTF-7.

reaction of nitrile groups can construct triazine rings. Up to now, CTFs from 1,4-dicyanobenzene (terephthalonitrile) gave high surface areas (over 3000 $m^2 g^{-1}$) only at high temperature, *i.e.*, heating to 400 °C for 20 h and then to 600 °C for 96 h.[18] Recently reported strong Brønsted acid conditions give lower surface areas (2 to 1152 $m^2 g^{-1}$) avoiding decomposition and condensation reactions such as C–H bond cleavage and carbonization.[27] Monomers 1,3-dicyanobenzene,[19] 1,4-dicyanobenzene,[13] 1,3,5-tricyanobenzene,[21] 1,2,4,5-tetracyanobenzene,[19] 4,4′-dicyanobiphenyl,[13] 4,4″-dicyanoterphenyl,[19] 2,6-dicyanopyridine,[19] tris(4-cyanophenyl)amine,[19] tris(4-cyanophenyl)benzene,[13] 2,5-dicyanothiophene,[13] 2,6-naphthalenedinitrile[20] and 5,5′-dicyanobipyridine[19] have already been utilized for CTF materials.

In contrast to strong Brønsted acids, ionothermal Lewis-acidic $ZnCl_2$ conditions offer significant advantages as being cheaper, experimentally simpler and by yielding materials with high surface areas. The synthesis of the new porous covalent triazine frameworks in Scheme 2 was carried out by following previously described procedures (see ESI†).[13,27] Here we used two different conditions to isolate these porous frameworks: Lewis acid condition ($ZnCl_2$) and strong Brønsted acid condition (CF_3SO_3H). A mixture of monomer (**M2–M4**) and $ZnCl_2$ in quartz ampoules was heated at 400 °C for 48 h. The crude product was stirred in water and diluted HCl for 24–48 h. The yields of PCTF-3 to -5 were around 85%. Alternatively, a clear solution of monomer (**M2–M4**) was added dropwise to the vigorously stirred CF_3SO_3H solution in dry $CHCl_3$ over 1 h at 0 °C under nitrogen, followed by stirring at room temperature for 12 h. After washing, the solid product (PCTF-6 and -7) was collected with good yield (greater than 80%). All attempts to polymerize **M4** under Brønsted acid conditions failed. The materials PCTF-3 to -7 are insoluble in common organic solvents. The formation of polytriazine frameworks was confirmed by FT-IR studies. The very strong intense characteristic carbonitrile stretching band of the monomers (**M2–M4**) around 2226 cm^{-1} disappeared or decreased significantly after reaction, and formed new characteristic C–N stretching bands for triazine units, at 1384 and 1508 cm^{-1} for PCTF-3 to PCTF-5; as well as 1366 and 1508 cm^{-1} for PCTF-6 to PCTF-7, respectively (see ESI† and Fig. 1).

As expected, PCTFs are amorphous in nature which is confirmed by powder X-ray diffraction studies (Fig. S2–S6, ESI†). Elemental analysis of PCTF-3 to PCTF-5 indicates nitrogen elimination during the polymerization reaction as reported previously.[18,23] It has been noticed that aromatic nitrile decomposition involves C–H and Ar–CN elimination. On the other hand, elemental analysis of PCTF-6 and PCTF-7 is close to theoretical values indicating better developed infinite triazine networks.

For applications of porous frameworks, it is important to consider their thermal stabilities. From thermogravimetric analysis (Fig. 2) decomposition of PCTFs starts only above 400 °C (Table S2, ESI†). We found that all PCTFs lose some small mass amount before the onset of decomposition due to the remaining hydrated water (Fig. 2, and Table S2†). PCTF-4 and PCTF-5 show the highest decomposition temperature of about 500 °C, which is comparable with other CTFs.

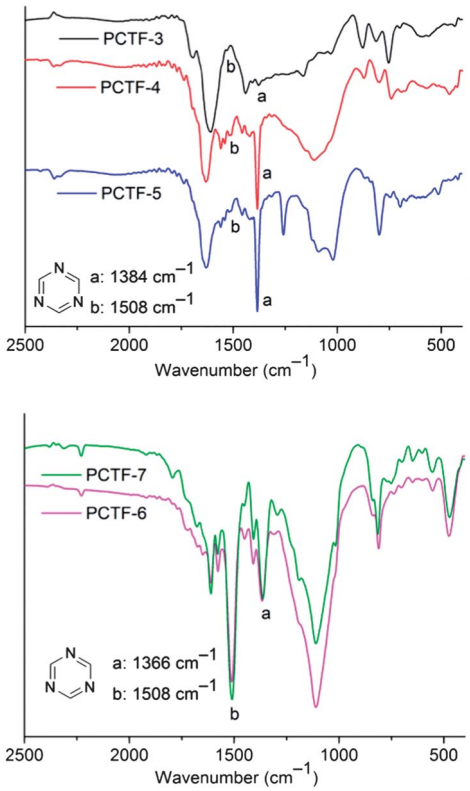

Fig. 1 FT-IR spectra of PCTF-3 to -5 (top) and PCTF-6 to -7 (bottom) confirming the formation of triazine units.

Frameworks PCTF-3 and 7 as well as PCTF-4 and -5 are each showing a similar surface morphology from scanning electron microscopy studies (Fig. 2) which is in line with their respective similar porosity characteristics from N_2 sorption studies (*cf.* Fig. 4a and Table 1). The SEM image of nonporous PCTF-6 shows larger particles (around 2 μm).

Gas sorption properties

The porosities of all PCTFs were characterized by N_2 sorption measurements as the accepted standard for surface area and pore size determination. All materials were activated by degassing at 200 °C for 24 h. Fig. 3 shows the N_2 adsorption/desorption isotherms of PCTF-3 to -7. A sharp adsorption/desorption step can be noticed at a low relative pressure (P/P_0) of 0 to 0.05 for PCTF-3 to -5 and PCTF-7. This is indicative of their substantial microporous character (pore widths < 2 nm, 20 Å, Table 1).[28] The adsorption isotherms of PCTF-3, -4, -5 and -7 follow a type-II character and the beginning of the almost linear middle section of the isotherm indicates the stage at which monolayer coverage is complete and multilayer adsorption takes place due to larger pores (see below).[28] The desorption of PCTF-3 and -7 exhibits a slight H4-type hysteresis, that is, the adsorption and desorption branch of the isotherm remain nearly horizontal and parallel over a wide range of P/P_0. Hysteresis appearing in the multilayer range of physisorption isotherms is usually associated with capillary condensation in mesopore structures. An H4-type hysteresis loop is often associated with narrow slit-like pores.

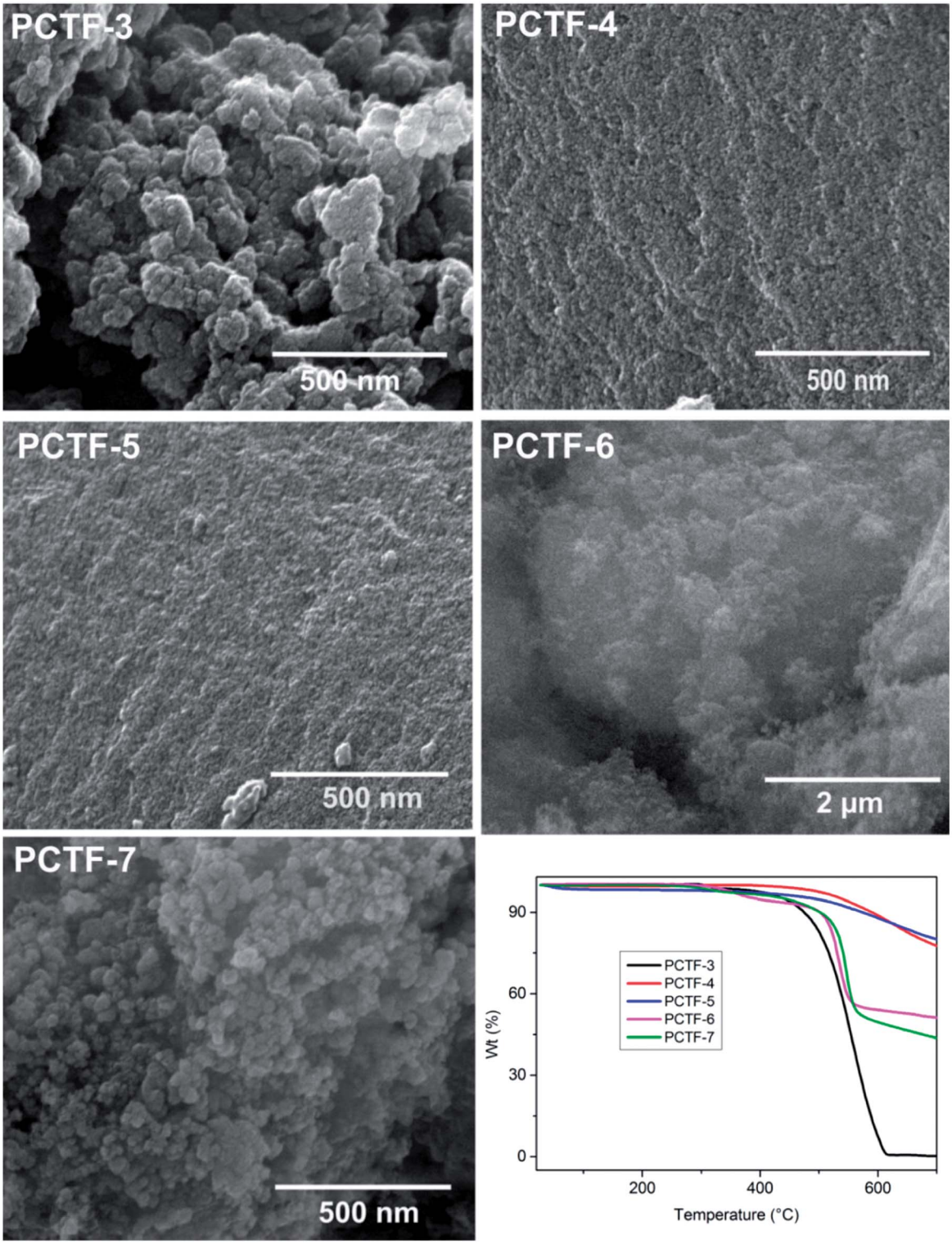

Fig. 2 Scanning electron micrographs and thermogravimetric analysis plots for PCTF-3 to -7.

The desorption of PCTF-4 and -5 shows an H2-type hysteresis loop which may be attributed to a difference in the mechanism between condensation and evaporation processes occurring in pores with narrow necks and wide cavities.[28] With PCTF-6 the isotherm is nearly type-III for an almost non-porous material. Its H3 loop which does not exhibit any limiting adsorption at high P/P_0 (Fig. 3) is observed with aggregates of plate-like particles giving rise to slit-shaped pores.[28]

The surface area is calculated by applying the Brunauer–Emmett–Teller (BET) model over the pressure range of $P/P_0 =$ 0.01–0.05 and the data are summarized in Table 1. Frameworks PCTF-3 and -7 as well as PCTF-4 and -5 which had a similar SEM

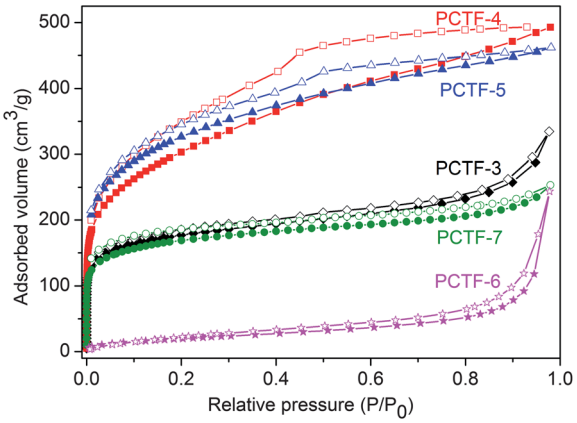

Fig. 3 Nitrogen adsorption–desorption isotherms (closed symbols for adsorption and open symbols for desorption).

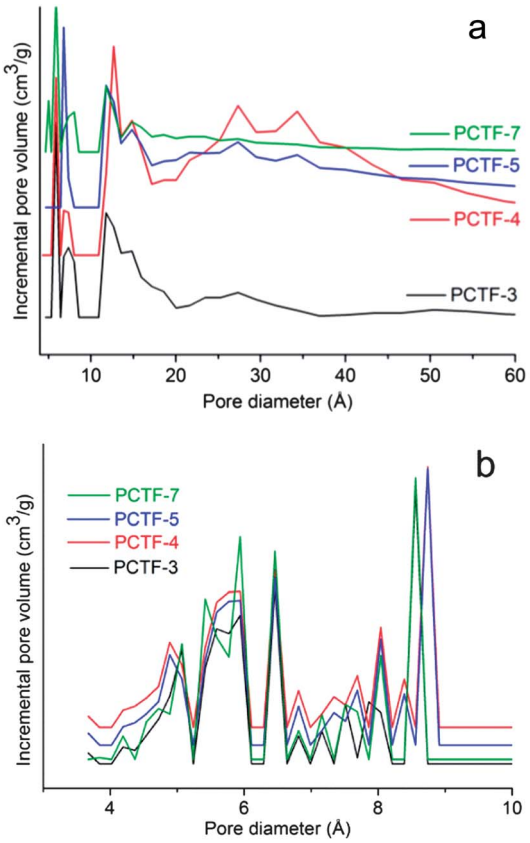

Fig. 4 NLDFT pore size distribution (PSD) curve of PCTFs from (a) N_2 adsorption (at 77 K) and (b) CO_2 adsorption (at 273 K) isotherms.

morphology are each showing comparable surface areas of ~620 and of ~1100 $m^2\ g^{-1}$, respectively. The surface area of PCTF-6 is low and essentially presents the outer surface area of a textured powder in line with the type-III adsorption isotherm. The obtained surface areas are comparable with other CTFs.[13,29,30] Even the frameworks PCTF-3 and -7 with an area of ~620 $m^2\ g^{-1}$ are also near the upper end when compared with other CTFs where surface areas range from 2 to 1152 $m^2\ g^{-1}$.[27] When comparing synthesis routes for the same monomer the Lewis acid ($ZnCl_2$) condition gives higher surface area materials (PCTF-3 and -5) than the strong Brønsted acid (CF_3SO_3H) condition (PCTF-6 and -7). Molten $ZnCl_2$ which is present in large excess (typically 10 : 1 molar ratio) not only acts as a Lewis acid and solvent but also as a pore-forming (porogen) or templating agent for the polymerization. From the comparison of the surface areas of PCTF-1 and -2 it becomes evident that the surface area and pore volume depend on the amount of $ZnCl_2$ porogen. The molar ratio of $ZnCl_2$ to tetranitrile was 10 : 1 and 5 : 1 for PCTF-1 and -2 (Scheme 1), respectively, which under otherwise identical conditions translated into a BET surface area of 2235 *versus* only 784 $m^2\ g^{-1}$ (Table 1). The more costly Brønsted acid (CF_3SO_3H) catalyst is applied in lower excess (about 4–5 : 1 molar ratio) and apparently lacks the porogenic properties. For Brønsted acid catalysis the porous network seems to depend much more on the underlying nitrile structure.

Table 1 Porosity data for PCTFs from N_2 isotherms at 77 K

Compound	S_{BET}[a] ($m^2\ g^{-1}$)	S_{Lang}[b] ($m^2\ g^{-1}$)	$V_{0.1}$[c] ($cm^3\ g^{-1}$)	V_{tot}[d] ($cm^3\ g^{-1}$)	$V_{0.1}/V_{tot}$	$V_{micro}(CO_2)$[e] ($cm^3\ g^{-1}$)
PCTF-1[f]	2235	2777	0.79	1.56	0.51	0.055
PCTF-2[f]	784	1313	0.29	0.76	0.38	0.040
PCTF-3	641	781	0.25	0.44	0.57	0.061
PCTF-4	1090	1299	0.41	0.75	0.55	0.052
PCTF-5	1183	1450	0.45	0.70	0.64	0.072
PCTF-6	79	135	—	—	—	—
PCTF-7	613	750	0.24	0.36	0.67	0.058

[a] Calculated BET surface area over the pressure range 0.01–0.05 P/P_0. [b] Langmuir surface area over the pressure range 0–110 Torr. [c] Micropore volume calculated from the N_2 adsorption isotherm at $P/P_0 = 0.1$ for pores with $d \leq 2$ nm (20 Å). [d] Total pore volume at $P/P_0 = 0.95$ for pores ≤20 nm. [e] Total pore volume for pores with $d \leq 1$ nm (10 Å, *cf.* Fig. 4b) from the CO_2 NL-DFT model at 273 K. [f] Data from ref. 23.

The pore size distribution (PSD) is a key factor characterizing porous materials. Non-local density functional theory (NLDFT) pore size distributions using a slit-pore model based on the N_2 adsorption isotherms of PCTFs yield pores with diameters less than 20 Å (2 nm) which correspond to micropores (Fig. 4). Micropores are expected in CTFs due to small rings and cages associated with triazine formation.[18,23] At the same time, broad pore-size distributions over 20 Å were observed especially for PCTF-4 and -5 due to additional mesopores present in the system. PSD curves show a larger fraction of pores with diameters over 20 Å for PCTF-4 and -5 than for PCTF-3 and -7 (Fig. 4). Moreover, from the N_2 sorption measurement at 77 K, the ratio of micropore volume to total pore volume ($V_{0.1}/V_{tot}$) can be calculated which describes the degree of microporosity (Table 1).[31] All PCTFs (except nonporous PCTF-6) exhibited $V_{0.1}/V_{tot}$ values above 0.5, ranging from 0.55 to 0.67, which indicates a high fraction and dominance of micropores in these frameworks.

Typically, the pore size distribution of a porous solid is evaluated from the analysis of N_2 adsorption isotherms measured at 77 K as was done above (*cf.* Fig. 4a). However, at such a cryogenic temperature diffusion of N_2 molecules into carbon micropores is very slow. Moreover, diffusion limitations

at this temperature might influence adsorption in ultramicropores (pores smaller than 7 Å).[32] For porous carbons which usually contain a wide range of pore sizes including ultramicropores, this would require time-consuming N_2 adsorption measurements and may still lead to under-equilibration of measured adsorption isotherms, which will give erroneous results of the analysis. For porous carbons problem of this type can be eliminated by using CO_2 adsorption analysis at 273 K.[33] The saturation pressure of CO_2 at 0 °C is very high (~26141 Torr), therefore low relative pressure measurements necessary for the micropore analysis are achieved in the range of moderate absolute pressures (1–760 Torr).[34] At 273 K and under higher absolute pressures CO_2 molecules can more easily access ultramicropores than N_2 at ~77 K and the kinetic diameter of CO_2 (3.3 Å) is also slightly smaller than for N_2 (3.64 Å). So, advantages of CO_2 micropore analysis at 273 K *versus* N_2 analysis at 77 K are: (i) faster analysis and (ii) greater confidence that measured adsorption points are equilibrated (both due to higher diffusion rates) and (iii) extension of the range of analysis to pores of smaller sizes that are accessible to CO_2 molecules but not to N_2.

Thus, from CO_2 adsorption isotherms at 273 K (see below), the pore size distribution was derived between 4 and 10 Å by using NLDFT with a "CO_2 on carbon based slit-pore" model (Fig. 4b). CO_2 adsorption with the NLDFT model yields a better resolved PSD towards the ultramicropore end than from N_2 adsorption isotherms (Fig. S7 to S9 in the ESI†). Here the four PCTFs (-3 to -5 and -7) give very similar pore size distributions for pores below 10 Å (1 nm) (Fig. 4b).

The porosity together with their stability makes PCTFs potential candidates for gas, especially hydrogen storage and carbon dioxide capture.[35–37] The H_2 sorption isotherms (Fig. 5a) yielded 1.03 to 1.24 wt% H_2 uptake at 77 K and 1 bar (Table 2). PCTF-5 showed the highest H_2 uptake (1.24 wt%) in line with its highest surface area and micropore volume among the adamantane-core PCTFs (Fig. S11 and S12 in ESI†). The H_2 uptake of PCTF-5 is comparable with other CTFs under similar conditions.[21,23] However, PCTF-3 and -7 with about half the BET surface area of PCTF-5 still show an H_2 uptake of about 1.04 wt %. The still high H_2 uptake can be correlated to a similar ultramicropore volume from CO_2 adsorption measurements $V_{micro}(CO_2)$ (Table 1) where the preferential adsorption of H_2 takes place due to higher heat of adsorption in small pores and channels.

Volumetric CO_2 and CH_4 sorption isotherms in Fig. 5b–d gave the CO_2 and CH_4 uptake capacities of PCTFs which are summarized in Table 2. CO_2 sorption was measured both at 273 K and 293 K (Fig. 5b and c). PCTF-5 has the highest CO_2 uptake capacity of 58 $cm^3\ g^{-1}$ at 273 K. These CO_2 uptake capacities around 50 $cm^3\ g^{-1}$ have to be compared to other CTFs which gave CO_2 uptakes of 20–93 $cm^3\ g^{-1}$ at 273 K and 1 bar.[21,27]

The CO_2 uptake capacity in PCTFs listed in Table 2 does not correlate with the heat of adsorption at zero coverage (see below) but with the BET surface area and pore volume (Table 1

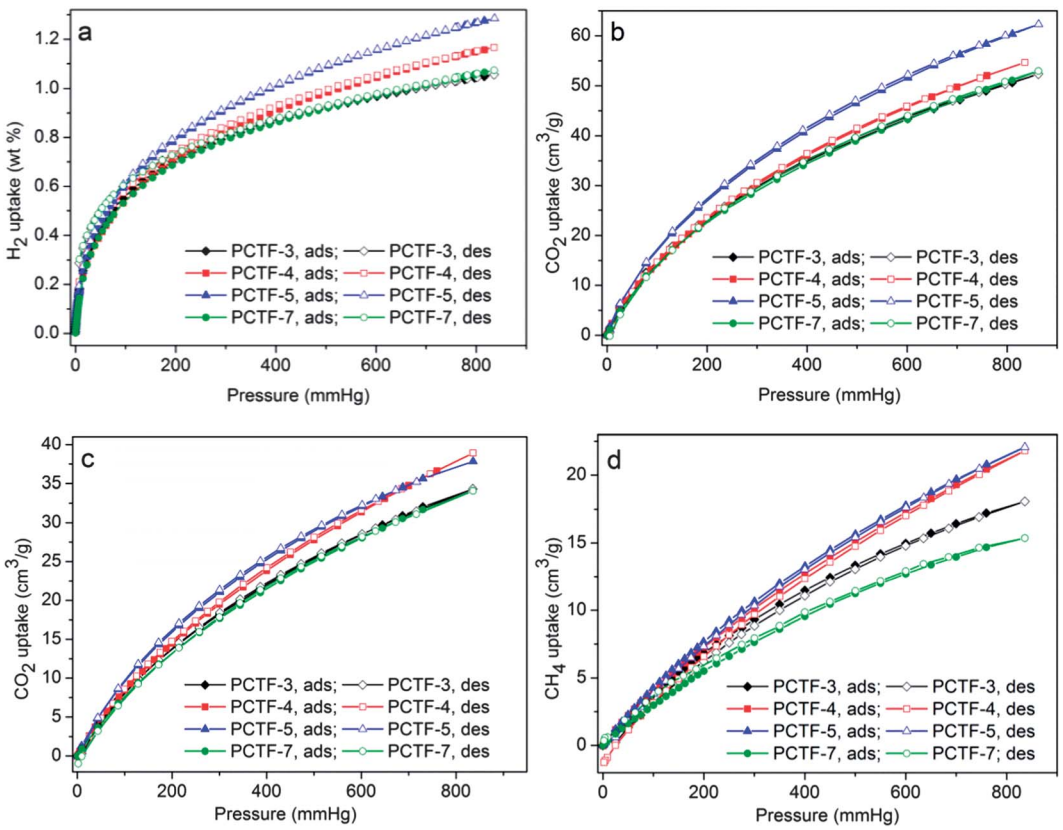

Fig. 5 Gas sorption isotherms (a) H_2 at 77 K, (b) CO_2 at 273 K, (c) CO_2 at 293 K, and (d) CH_4 at 273 K.

Table 2 Gas sorption at 1 bar, heat of adsorption for CO_2 at zero coverage and selectivity of PCTFs for $p \rightarrow 0$

Compound	H_2[a] (wt%)	CO_2[b] ($cm^3\ g^{-1}$)	CO_2[c] ($cm^3\ g^{-1}$)	$Q^0_{ads}(CO_2)$[d] (kJ mol^{-1})	N_2[b] ($cm^3\ g^{-1}$)	CH_4[b] ($cm^3\ g^{-1}$)	CO_2:N_2	CO_2:CH_4 selectivity[e]	CH_4:N_2
PCTF-1	1.86	73.0	44.9	30[f]	7.8	23.6	14 : 1	5 : 1	3 : 1[f]
PCTF-2	0.90	41.5	24.2	26[f]	7.3	15.1	14 : 1	5 : 1	3 : 1[f]
PCTF-3	1.03	48.7	32.4	27	5.9	17.1	25 : 1	6 : 1	5 : 1
PCTF-4	1.13	51.6	36.3	28	5.7	20.2	26 : 1	6 : 1	5 : 1
PCTF-5	1.24	58.1	36.1	27	7.0	20.5	32 : 1	7 : 1	5 : 1
PCTF-7	1.04	48.9	32.2	25	1.6	14.6	41 : 1	7 : 1	6 : 1

[a] Uptake at 77 K. [b] Uptake at 273 K. [c] Uptake at 293 K. [d] Heat of adsorption for CO_2 at zero loading from adsorption isotherms acquired at 273 and 293 K using Virial fits with the Clausius–Clapeyron eqn (1) *cf.* Fig. 7 and S10. [e] The ideal selectivity (selectivity for $p \rightarrow 0$) was calculated using the IAST method from the ratios of the Henry-constants which were derived from maximum adsorbed amount (saturation parameter in the Toth-equation) and the affinity constant (see Tables S4 and S5 in the ESI). For gas selectivities calculated at 273 K from the initial slopes in the Henry region see Fig. S15 and Table S6 in the ESI. [f] Data calculated here in this work from the data reported in ref. 23.

and Fig. S11 to S13†). For PCTF-7 having the lowest BET surface area and $V_{0.1}$ in the series the still sizable CO_2 uptake can be ascribed to effects of the strong quadrupolar interactions of CO_2 with the large amount of nitrogen atoms (Table S1 in the ESI†) still present on the pore surface.

The CH_4 adsorption of the PCTFs was investigated at low pressure (up to 1 bar) and 273 K. The CH_4 uptake capacities of PCTF-3 to -7 are between 14 and 20 $cm^3\ g^{-1}$ which are comparable with the values for PCTF-1 and -2 from our previous work (included in Table 2).[23] For CTFs no other CH_4 sorption data have been recorded yet in the literature to the best of our knowledge. The gas sorption capacity for CH_4 (Table 2) of PCTFs follows again the increase in surface area and pore volume (Table 1, Fig. S11 to S13†).

Overall, the H_2, CO_2 and CH_4 gas uptake capacities of PCTF-1 to -7 (excluding non-porous PCTF-6) largely increase with the surface area and pore volume (Fig. S11 to S13 in the ESI†). Thereby the micropore volume gives a slightly better correlation than the total pore volume which can be explained by the preferential gas adsorption in small pores and channels due to higher heat of adsorption. It is noteworthy that PCTF-2 (from tetra(4-cyanophenyl)ethylene obtained at a 1 : 5 molar ratio with $ZnCl_2$, *cf.* Scheme 1) also deviates from the gas uptake–porosity correlation. The uptake for all three gases is too low due to its available surface area and pore volume. We ascribe this to the significantly lower micropore fraction ($V_{0.1}/V_{tot}$) or ultramicropore volume ($V_{micro}(CO_2)$) (Table 1) which in turn is evidence of a different microstructure.

Furthermore, the highest H_2, CO_2 and CH_4 gas uptakes are given by PCTF-1 and -5 from the tetrakis(4-cyanophenyl) monomers **M1** and **M4**, followed by PCTF-4 from tris(4-cyanophenyl) monomer **M3** (*cf.* Schemes 1 and 2, Table 2 and Fig. S11–S13†). This points to the importance of increasing the fraction of polarizing adsorption sites in CTFs for higher gas uptake through a higher number of nitrile groups in the monomer starting materials.

From the available single-gas adsorption isotherms, the selectivity in the adsorption of CO_2 and CH_4 from CO_2–N_2, CO_2–CH_4 and CH_4–N_2 gas mixtures was evaluated by the ideal adsorption solution theory (IAST) which is often used to predict gas mixture adsorption behavior in porous materials.[38,39] Alternatively, the ratio of the initial slopes in the Henry region (0–0.12 bar) of the adsorption isotherms (Fig. S15 in the ESI†)[40,41] can be used to determine the gas selectivities exhibited by the PCTFs (Table S6†). The selectivity does not depend only on the size of the gas components (kinetic diameter: CO_2 3.3 Å, N_2 3.64 Å and CH_4 3.8 Å) but also on the polarizability of the surface and of the gas components.

The theoretical gas selectivities for CO_2 over N_2 and CO_2 over CH_4 derived from the IAST model (Table 2 and Fig. 6) can be ascribed to the combined effects of the size of the pore apertures and the strong quadrupolar interactions of CO_2 with

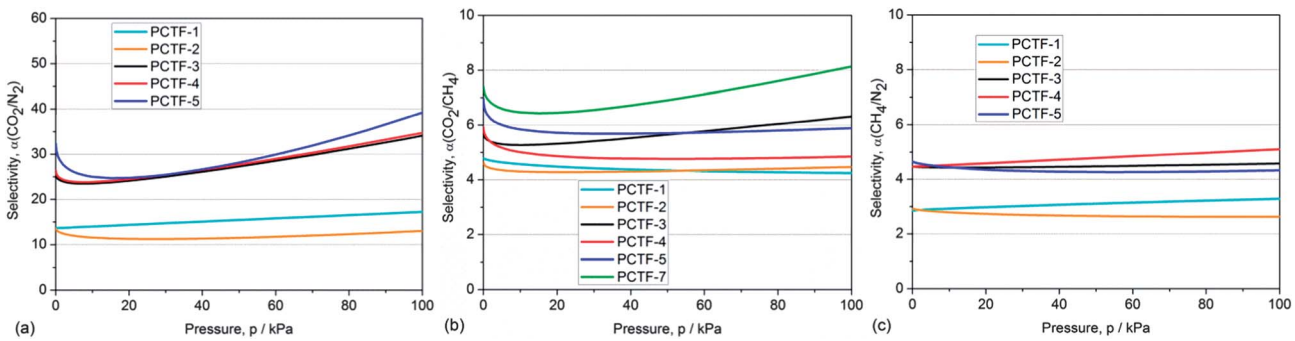

Fig. 6 IAST-predicted adsorption selectivity from an equimolar (a) CO_2–N_2, (b) CO_2–CH_4 and (c) CH_4–N_2 gas mixtures at 273 K for PCTFs. IAST calculations for PCTF-7 involving N_2 are shown only in Fig. S14 in the ESI† because of low accuracy due to the low N_2 loading of this compound.

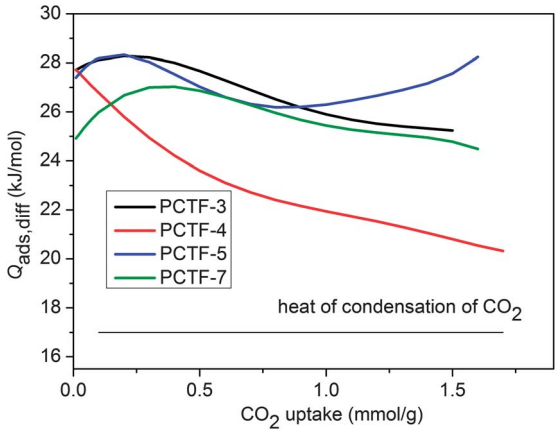

Fig. 7 Isosteric differential heat of adsorption ($Q_{ads,diff}$) as a function of CO_2 uptake for PCTF-3 to -5 and PCTF-7. The intermediate maximum for PCTF-3, -5 and -7 around 0.25 mmol g^{-1} is within the standard deviations for $Q_{ads,diff}$.

nitrogen atoms present on the pore surface. The higher quadrupole moment of CO_2 (CO_2: 14.3×10^{-40} cm^2, N_2: 4.65×10^{-40} cm^2; CH_4: none)[42] leads to a stronger electrostatic interaction with the framework. PCTF-3 to -5 show a high and similar CO_2:N_2 selectivity of 25 to 32 for $p \rightarrow 0$ at 273 K (Table 2). The obtained ratios are comparable with other CTFs.[23,27] The CO_2:N_2 selectivity is the highest for PCTF-7 with 41 : 1 which is in line with the above argument of strong quadrupolar interactions of CO_2 with the largest amount of nitrogen atoms (Table S1 in the ESI†) still present on the pore surface in this PCTF. Following a small decrease the selectivities for CO_2 over N_2 increase significantly with pressure for PCTF-3 to -5 to values of 34–39 at $p = 100$ kPa (Fig. 6). Cooper *et al.* calculated CO_2:N_2 selectivities for various CTFs mainly between 14 and 24 : 1 at 273 K using IAST.[27] The CO_2:CH_4 selectivities of PCTFs are found here as 5–7 : 1 for $p \rightarrow 0$ at 273 K (Table 2). The CH_4:N_2 selectivities for PCTF-3 to -5 are ~5 : 1 for $p \rightarrow 0$ at 273 K (Table 2). Recently, Zhu *et al.* published PAF-26 materials which have selectivities for CH_4 over N_2 in the range of 4.2 to 6.5 based on single gas adsorption isotherms using the IAST model.[43] CH_4 adsorbs preferentially over N_2 due to its higher polarizability (average electric dipole polarizabilities: CO_2: 2.911×10^{-24} cm^3, N_2: 1.7403×10^{-24} cm^3 and CH_4: 2.593×10^{-24} cm^3).[23,44]

Overall, there is no loss in CO_2 selectivity over N_2 and CH_4 and also in CH_4 selectivity over N_2. There can even be an increase in selectivity with total pressure, which is most evident for CO_2 over N_2 with PCTF-3 to -5 and for CO_2 over CH_4 with PCTF-3 and -7. Such increasing CO_2 selectivities may be explained by a collective effect of the progressive CO_2 adsorption onto the active nitrogen sites.

From two adsorption isotherms acquired at different temperatures T_1 and T_2 (*cf.* Fig. 5b and c), the differential heat of adsorption (negative adsorption enthalpy) $Q_{ads,diff}$ can be calculated for any amount of adsorbed substance after determining the required relative pressures p_1 and p_2. A virial equation was used to correlate the experimental data and to calculate the isosteric heats of adsorption and the limiting heats of adsorption at zero loading[45] with a modified form of the Clausius–Clapeyron equation (eqn (1)).[46] $Q_{ads,diff}$ was calculated over the whole adsorption range from the 273 K and 293 K isotherms for CO_2 in PCTF-3 to -5 and PCTF-6 (Fig. 7). The heat of adsorption at zero loading Q^0_{ads} is included in Table 2.

$$Q_{ads,diff} = -R \ln\left(\frac{p_2}{p_1}\right) \frac{T_1 T_2}{T_2 - T_1} \quad (1)$$

At zero-loading the Q^0_{ads} values for PCTF-3 to -5 and CTF-7 are 30–25 kJ mol^{-1} (Table 2) and then drop at higher loading. Yet, the heat of CO_2 adsorption for PCTFs stays well above the heat of liquefaction of bulk CO_2 with 17 kJ mol^{-1} (ref. 47) or around the isosteric enthalpy of adsorption for CO_2 on activated carbons (*e.g.* BPL: 25.7 kJ mol^{-1}, A10: 21.6 kJ mol^{-1}, and Norit R1 Extra: 22.0 kJ mol^{-1}).[48] The high adsorption enthalpy at low coverage is explained by the initial filling of the small ultramicropores up to 4 Å with adsorbate–surface interactions to either sides or ends of the CO_2 molecules.[11] Careful evaluation of the performance of a given porous material should consider the heat of adsorption over the entire adsorption range (not just at zero coverage). At zero to low coverage the magnitude of the isosteric heat of adsorption is largely a function of the binding strength of the strongest binding sites within the material. Frameworks bearing CO_2-interacting functionalities or highly polarizing adsorption sites display the highest values. PCTF-4 exhibits the steepest drop in $Q_{ads,diff}$ with CO_2 loading, its high energy sites are rapidly saturated already at low CO_2 uptake.

We note that the small maximum in $Q_{ads,diff}$ seen between 0 and 0.5 mmol g^{-1} CO_2 uptake is still within the error margin of at least ±3 kJ mol^{-1} which we calculated on average for $Q_{ads,diff}$ data points.[49] Consequently Q^0_{ads} values should only be reported with significant digits before the decimal point. If Q_{ads} would indeed exhibit relative maxima as a function of CO_2 uptake, this means that a simultaneous, exothermic process must take place in this range. A possible exothermic process, which is not easy to detect, is the rearrangement of already adsorbed CO_2 molecules towards a closer, energetically more favorable configuration.

Conclusions

A series of 4-cyanophenyl-substituted adamantanes as newly introduced building blocks with varying symmetry (T_d, C_{3v} and C_{2v}) and functional group density was used for comparative investigation of porous covalent triazine-based frameworks (PCTFs) which were obtained under conditions employing Lewis acid ($ZnCl_2$) catalysis and strong Brønsted acid (CF_3SO_3H) catalysis. FT-IR spectra confirm the triazine ring formation in the obtained PCTFs. These PCTFs are stable up to 450 °C, exhibit substantial microporous character ($V_{0.1}/V_{tot}$ >0.5) and have BET surface areas between 600 and 1200 m^2 g^{-1} which is similar to other known CTFs. The surface area, porosity and micropore volume are higher in the case of $ZnCl_2$ catalyzed conditions compared to strong Brønsted acid conditions and increase with the number of 4-cyanophenyl groups and symmetry of the building blocks. Porosity was determined from standard N_2 adsorption isotherms and in addition the ultramicropore size distribution between 4 and 10 Å was derived by using NLDFT with a "CO_2 on carbon based slit-pore model". Based on gas

sorption studies (N_2, H_2, CO_2 and CH_4), these porous frameworks preferentially adsorb CO_2 over N_2 and CH_4. The PCTF from 1,3,5,7-tetrakis(4-cyanophenyl)adamantane (with $ZnCl_2$) gave the highest surface area and highest gas uptake capacities (*e.g.* for CO_2 58.1 $cm^3\ g^{-1}$ at 273 K) with the material from 1,3,5-tris(4-cyanophenyl)adamantane following close behind. High ratios for the CO_2:N_2 and CO_2:CH_4 selectivities (up to 41 : 1 and 6 : 1, respectively, at 273 K) were found for these adamantane-based PCTFs. Together with the PCTF from tetrakis(4-cyanophenyl)ethylene this study suggests to increase the number of nitrile groups in the underlying monomers to advance the gas uptake in the resulting frameworks.

An *a priori* question concerned the factors symmetry and density of functional groups. Is there an advantage of a highly symmetric tetrahedral building block over a lower symmetric trigonal or bent building block with a lower density of functional groups? This question is answered here that both symmetry and density of functional groups have approximately equal importance, as seen from the slightly better results demonstrated by the tetrahedral block. This answer might be of general significance for COFs obtained under non-reversible conditions. For COFs obtained under reversible conditions the difference might be more emphasized and its assessment is a matter of future research.

Acknowledgements

IB thanks the Alexander-von-Humboldt foundation for a post-doctoral fellowship.

Notes and references

1 X. Zhou, H. Ren and G. Zhu, *Chem. Commun.*, 2013, **49**, 3925–3936; S.-Y. Ding and W. Wang, *Chem. Soc. Rev.*, 2013, **42**, 548–568; Y. Jin, Y. Zhu and W. Zhang, *CrystEngComm*, 2013, **15**, 1484–1499; Z. Xiang and D. Cao, *J. Mater. Chem. A*, 2013, **1**, 2691–2718; H. A. Patel, F. Karadas, J. Byun, J. Park, E. Deniz, A. Canlier, Y. Jung, M. Atilhan and C. T. Yavuz, *Adv. Funct. Mater.*, 2013, **23**, 2270–2276; Y. Zhu, H. Long and W. Zhang, *Chem. Mater.*, 2013, **25**, 1630–1635; N. B. McKeown and P. M. Budd, *Macromolecules*, 2010, **43**, 5163–5176; R. Dawson, A. I. Cooper and D. J. Adams, *Prog. Polym. Sci.*, 2012, **37**, 530–563; J. Germain, J. M. J. Fréchet and F. Svec, *Small*, 2009, **5**, 1098–1111; P. Kaur, J. T. Hupp and S. T. Nguyen, *ACS Catal.*, 2011, **1**, 819–835; U. H. F. Bunz, *Chem. Rev.*, 2000, **100**, 1605–1644.

2 M. G. Rabbani and H. M. El-Kaderi, *Chem. Mater.*, 2012, **24**, 1511–1517.

3 A. P. Côté, A. I. Benin, N. W. Ockwig, M. O'Keeffe, A. J. Matzger and O. M. Yaghi, *Science*, 2005, **310**, 1166–1170; S. Wan, J. Guo, J. Kim, H. Ihee and D. L. Jiang, *Angew. Chem., Int. Ed.*, 2008, **47**, 8826–8830.

4 R. W. Tilford, W. R. Gemmill, H. C. zur Loye and J. J. Lavigne, *Chem. Mater.*, 2006, **18**, 5296–5301; W. Lu, D. Yuan, D. Zhao, C. I. Schilling, O. Plietzsch, T. Muller, S. Bräse, J. Guenther, J. Blümel, R. Krishna, Z. Li and H. C. Zhou, *Chem. Mater.*, 2010, **22**, 5964–5972; F. J. Uribe-Romo, J. R. Hunt, H. Furukawa, C. Klock, M. O'Keeffe and O. M. Yaghi, *J. Am. Chem. Soc.*, 2009, **131**, 4570–4572.

5 (*a*) H. M. El-Kaderi, J. R. Hunt, J. L. Mendoza-Cortes, A. P. Côté, R. E. Taylor, M. O'Keeffe and O. M. Yaghi, *Science*, 2007, **316**, 268–272; (*b*) S. Kandambeth, A. Mallick, B. Lukose, M. V. Mane, T. Heine and R. Banerjee, *J. Am. Chem. Soc.*, 2012, **134**, 19524–19527.

6 L. M. Lanni, R. W. Tilford, M. Bharathy and J. J. Lavigne, *J. Am. Chem. Soc.*, 2011, **133**, 13975–13983.

7 E. L. Spitler, M. R. Giovino, S. L. White and W. R. Dichtel, *Chem. Sci.*, 2011, **2**, 1588–1593.

8 J. Germain, J. Hradil, J. M. J. Fréchet and F. Svec, *Chem. Mater.*, 2006, **18**, 4430–4435.

9 B. S. Ghanem, K. J. Msayib, N. B. McKeown, K. D. M. Harris, Z. Pan, P. M. Budd, A. Butler, J. Selbie, D. Book and A. Walton, *Chem. Commun.*, 2007, 67–69.

10 T. Ben, H. Ren, S. Ma, D. Cao, J. Lan, X. Jing, W. Wang, J. Xu, F. Deng, J. M. Simmons, S. Qiu and G. Zhu, *Angew. Chem., Int. Ed.*, 2009, **48**, 9457–9460.

11 H. Zhao, Z. Jin, H. Su, J. Zhang, X. Yao, H. Zhao and G. Zhu, *Chem. Commun.*, 2013, **49**, 2780–2782.

12 J.-X. Jiang, F. Su, A. Trewin, C. D. Wood, N. L. Campbell, H. Niu, C. Dickinson, A. Y. Ganin, M. J. Rosseinsky, Y. Z. Khimyak and A. I. Cooper, *Angew. Chem., Int. Ed.*, 2007, **46**, 8574–8578.

13 P. Kuhn, M. Antonietti and A. Thomas, *Angew. Chem., Int. Ed.*, 2008, **47**, 3450–3453.

14 M. G. Rabbani, T. E. Reich, R. M. Kassab, K. T. Jackson and H. M. El-Kaderi, *Chem. Commun.*, 2012, **48**, 1141–1143.

15 M. G. Rabbani and H. M. El-Kaderi, *Chem. Mater.*, 2011, **23**, 1650–1653.

16 J.-Y. Lee, C. D. Wood, D. Bradshaw, M. J. Rosseinsky and A. I. Cooper, *Chem. Commun.*, 2006, 2670–2672.

17 C. F. Martin, E. Stockel, R. Clowes, D. J. Adams, A. I. Cooper, J. J. Pis, F. Rubiera and C. Pevida, *J. Mater. Chem.*, 2011, **21**, 5475–5483.

18 P. Kuhn, A. l. Forget, D. Su, A. Thomas and M. Antonietti, *J. Am. Chem. Soc.*, 2008, **130**, 13333–13337.

19 P. Kuhn, A. Thomas and M. Antonietti, *Macromolecules*, 2009, **42**, 319–326.

20 M. J. Bojdys, J. Jeromenok, A. Thomas and M. Antonietti, *Adv. Mater.*, 2010, **22**, 2202–2205.

21 P. Katekomol, J. Roeser, M. Bojdys, J. Weber and A. Thomas, *Chem. Mater.*, 2013, **25**, 1542–1548.

22 C. E. Chan-Thaw, A. Villa, P. Katekomol, D. Su, A. Thomas and L. Prati, *Nano Lett.*, 2010, **10**, 537–541.

23 A. Bhunia, V. Vasylyeva and C. Janiak, *Chem. Commun.*, 2013, **49**, 3961–3963.

24 W. Zhang, F. Liang, C. Li, L.-G. Qiu, Y.-P. Yuan, F.-M. Peng, X. Jiang, A.-J. Xie, Y.-H. Shen and J.-F. Zhu, *J. Hazard. Mater.*, 2011, **186**, 984–990.

25 Introduction to the themed issue on porous carbon materials: A.-H. Lu and S. Dai, *J. Mater. Chem. A*, 2013, **1**, 932.

26 J. R. Morris, C. I. Contescu, M. F. Chisholm, V. R. Cooper, J. Guo, L. He, Y. Ihm, E. Mamontov, Y. B. Melnichenko, R. J. Olsen, S. J. Pennycook, M. B. Stone, H. Zhang and N. C. Gallego, *J. Mater. Chem. A*, 2013, **1**, 9341–9350; Y. Xia,

Z. Yang and Y. Zhu, *J. Mater. Chem. A*, 2013, **1**, 9365–9381; N. Fechler, S.-A. Wohlgemuth, P. Jäker and M. Antonietti, *J. Mater. Chem. A*, 2013, **1**, 9418–9421; S. J. Yang, J. H. Kang, H. Jung, T. Kim and C. R. Park, *J. Mater. Chem. A*, 2013, **1**, 9427–9432; L. Huang and D. Cao, *J. Mater. Chem. A*, 2013, **1**, 9433–9439.

27 S. Ren, M. J. Bojdys, R. Dawson, A. Laybourn, Y. Z. Khimyak, D. J. Adams and A. I. Cooper, *Adv. Mater.*, 2012, **24**, 2357–2361.

28 (*a*) K. S. W. Sing, D. H. Everett, R. A. W. Haul, L. Moscou, R. A. Pierotti, J. Rouquerol and T. Siemieniewska, *Pure Appl. Chem.*, 1985, **57**, 603–619; (*b*) M. Thommes, B. Smarsly, M. Groenewolt, P. I. Ravikovitch and A. V. Neimark, *Langmuir*, 2006, **22**, 756–764.

29 H. Ren, T. Ben, E. Wang, X. Jing, M. Xue, B. Liu, Y. Cui, S. Qiu and G. Zhu, *Chem. Commun.*, 2010, **46**, 291–293.

30 R. Palkovits, M. Antonietti, P. Kuhn, A. Thomas and F. Schüth, *Angew. Chem., Int. Ed.*, 2009, **48**, 6909–6912.

31 R. Dawson, A. Laybourn, R. Clowes, Y. Z. Khimyak, D. J. Adams and A. I. Cooper, *Macromolecules*, 2009, **42**, 8809–8816.

32 F. Rodriguez-Reinoso and A. Linares-Solano, in *Chemistry and Physics of Carbon*, ed. P. A. Thrower, Marcel Dekker, New York, 1988, vol. 21.

33 J. Garrido, A. Linares-Solano, J. M. Martin-Martinez, M. Molina-Sabio, F. Rodriguez-Reinoso and R. Torregosa, *Langmuir*, 1987, **3**, 76; D. Cazorla-Amoros, J. Alcaniz-Monje and A. Linares-Solano, *Langmuir*, 1996, **12**, 2820; J. Garcia-Martinez, D. Cazorla-Amoros and A. Linares-Solano, in *Characterization of Porous Solids V*, ed. K. K. Unger, G. Kreysa and J. P. Baselt, Elsevier, Amsterdam, 2000, pp. 485–494.

34 Quantachrome Instruments (1900 Corporate Drive, Boynton Beach, FL 33426 USA, http://www.quantachrome.com) Powder Tech Note 35.

35 L. Schlapbach and A. Züttel, *Nature*, 2001, **414**, 353–358.

36 D. Zhao, D. Q. Yuan and H. C. Zhou, *Energy Environ. Sci.*, 2008, **1**, 222–235.

37 U. Eberle, M. Felderhoff and F. Schüth, *Angew. Chem., Int. Ed.*, 2009, **48**, 6608–6630.

38 A. L. Myers and J. M. Prausnitz, *AIChE J.*, 1965, **11**, 121–127; J. Toth, *Adv. Colloid Interface Sci.*, 1995, **55**, 1–239.

39 J. Möllmer, A. Möller, C. Patzschke, K. Stein, D. Lässig, J. Lincke, R. Gläser, H. Krautscheid and R. Staudt, *J. Mater. Chem.*, 2012, **22**, 10274–10286; F. Debatin, J. Möllmer, S. S. Mondal, K. Behrens, A. Möller, R. Staudt, A. Thomas and H.-J. Holdt, *J. Mater. Chem.*, 2012, **22**, 10221–10227.

40 V. Abetz, T. Brinkmann, M. Dijkstra, K. Ebert, D. Fritsch, K. Ohlrogge, D. Paul, K. V. Peinemann, S. Pereira-Nunes, N. Scharnagl and M. Schossig, *AIChE J.*, 2006, **8**, 328–358.

41 Y.-S. Bae, O. K. Farha, A. M. Spokoyny, C. A. Mirkin, J. T. Hupp and R. Q. Snurr, *Chem. Commun.*, 2008, 4135–4137.

42 C. Graham, D. A. Imrie and R. E. Raab, *Mol. Physics*, 1998, **93**, 49–56.

43 H. Ma, H. Ren, X. Zou, S. Meng, F. Sun and G. Zhu, *Polym. Chem.*, 2014, DOI: 10.1039/c3py00647f, in press.

44 D. R. Lide, *CRC Handbook of Chemistry and Physics*, CRC Press, Boca Raton, FL, 2009, Table 4, pp. 10–196.

45 C. L. Cavalcante, Jr and D. M. Ruthven, *Ind. Eng. Chem. Res.*, 1995, **34**, 177–184; M. S. Sun, D. B. Shah, H. H. Xu and O. Talu, *J. Phys. Chem. B*, 1998, **102**, 1466–1473.

46 F. Rouquerol, J. Rouquerol and K. Sing, *Adsorption by powders and porous solids*, F. Rouquerol, J. Rouquerol and K.Sing, ed. Academic Press, San Diego, 1999, vol. 11.

47 S. Keskin, T. M. van Heest and D. S. Sholl, *ChemSusChem*, 2010, **3**, 879–891.

48 S. Himeno, T. Komatsu and S. Fujita, *J. Chem. Eng. Data*, 2005, **50**, 369–376; K. B. Lee, M. G. Beaver, H. S. Caram and S. Sircar, *Ind. Eng. Chem. Res.*, 2008, **47**, 8048–8062.

49 F. Jeremias, A. Khutia, S. K. Henninger and C. Janiak, *J. Mater. Chem.*, 2012, **22**, 10148–10151; F. Jeremias, V. Lozan, S. Henninger and C. Janiak, *Dalton Trans.*, 2013, **42**, 15967–15973.